Publication V

T. Näsi, H. Mäki, P. Hiltunen, J. Heiskala, I. Nissilä, K. Kotilahti, and R. J. Ilmoniemi. Effect of task-related extracerebral circulation on diffuse optical tomography: experimental data and simulations on the forehead. *Biomedical Optics Express*, 4:412–426, Mar 2013.

Biomedical Optics EXPRESS

Effect of task-related extracerebral circulation on diffuse optical tomography: experimental data and simulations on the forehead

Tiina Näsi,[1,2,*] Hanna Mäki,[1,2] Petri Hiltunen,[1] Juha Heiskala,[3] Ilkka Nissilä,[1,2] Kalle Kotilahti,[1,2] and Risto J. Ilmoniemi[1,2]

[1]*Department of Biomedical Engineering and Computational Science (BECS), Aalto University School of Science, P.O. Box 12200, FI-00076 AALTO, Espoo, Finland*
[2]*BioMag Laboratory, HUS Medical Imaging Center, Helsinki University Central Hospital, P.O. Box 340, FI-00029 HUS, Finland*
[3]*Department of Computer Science, University College London, Gower Street, London WC1E 6BT, United Kingdom*
**tiina.nasi@aalto.fi*

Abstract: The effect of task-related extracerebral circulatory changes on diffuse optical tomography (DOT) of brain activation was evaluated using experimental data from 14 healthy human subjects and computer simulations. Total hemoglobin responses to weekday-recitation, verbal-fluency, and hand-motor tasks were measured with a high-density optode grid placed on the forehead. The tasks caused varying levels of mental and physical stress, eliciting extracerebral circulatory changes that the reconstruction algorithm was unable to fully distinguish from cerebral hemodynamic changes, resulting in artifacts in the brain activation images. Crosstalk between intra- and extracranial layers was confirmed by the simulations. The extracerebral effects were attenuated by superficial signal regression and depended to some extent on the heart rate, thus allowing identification of hemodynamic changes related to brain activation during the verbal-fluency task. During the hand-motor task, the extracerebral component was stronger, making the separation less clear. DOT provides a tool for distinguishing extracerebral components from signals of cerebral origin. Especially in the case of strong task-related extracerebral circulatory changes, however, sophisticated reconstruction methods are needed to eliminate crosstalk artifacts.

OCIS codes: (170.0110) Imaging systems; (170.1470) Blood or tissue constituent monitoring; (170.3880) Medical and biological imaging; (170.6960) Tomography.

References and links

1. E. Kirilina, A. Jelzow, A. Heine, M. Niessing, H. Wabnitz, R. Brühl, B. Ittermann, A. M. Jacobs, and I. Tachtsidis, "The physiological origin of task-evoked systemic artefacts in functional near infrared spectroscopy," Neuroimage **61**(1), 70–81 (2012).
2. P. D. Drummond, "Adrenergic receptors in the forehead microcirculation," Clin. Auton. Res. **6**(1), 23–27 (1996).
3. P. D. Drummond, "The effect of adrenergic blockade on blushing and facial flushing," Psychophysiology **34**(2), 163–168 (1997).
4. L. Minati, I. U. Kress, E. Visani, N. Medford, and H. D. Critchley, "Intra- and extra-cranial effects of transient blood pressure changes on brain near-infrared spectroscopy (NIRS) measurements," J. Neurosci. Methods **197**(2), 283–288 (2011).
5. I. Tachtsidis, T. S. Leung, A. Chopra, P. H. Koh, C. B. Reid, and C. E. Elwell, "False positives in functional near-infrared topography," Adv. Exp. Med. Biol. **645**, 307–314 (2009).
6. T. Takahashi, Y. Takikawa, R. Kawagoe, S. Shibuya, T. Iwano, and S. Kitazawa, "Influence of skin blood flow on near-infrared spectroscopy signals measured on the forehead during a verbal fluency task," Neuroimage **57**(3), 991–1002 (2011).
7. M. A. Franceschini, D. K. Joseph, T. J. Huppert, S. G. Diamond, and D. A. Boas, "Diffuse optical imaging of the whole head," J. Biomed. Opt. **11**(5), 054007 (2006).
8. S. R. Arridge, "Optical tomography in medical imaging," Inverse Probl. **15**(2), R41–R93 (1999).
9. A. Gibson and H. Dehghani, "Diffuse optical imaging," Philos. Transact. A Math. Phys. Eng. Sci. **367**(1900), 3055–3072 (2009).

#178634 - $15.00 USD Received 26 Oct 2012; revised 28 Jan 2013; accepted 7 Feb 2013; published 13 Feb 2013

10. B. W. Zeff, B. R. White, H. Dehghani, B. L. Schlaggar, and J. P. Culver, "Retinotopic mapping of adult human visual cortex with high-density diffuse optical tomography," Proc. Natl. Acad. Sci. U.S.A. **104**(29), 12169–12174 (2007).
11. N. M. Gregg, B. R. White, B. W. Zeff, A. J. Berger, and J. P. Culver, "Brain specificity of diffuse optical imaging: improvements from superficial signal regression and tomography," Front Neuroenergetics **2**, 14 (2010).
12. S. P. Koch, C. Habermehl, J. Mehnert, C. H. Schmitz, S. Holtze, A. Villringer, J. Steinbrink, and H. Obrig, "High-resolution optical functional mapping of the human somatosensory cortex," Front Neuroenergetics **2**, 12 (2010).
13. C. Habermehl, S. Holtze, J. Steinbrink, S. P. Koch, H. Obrig, J. Mehnert, and C. H. Schmitz, "Somatosensory activation of two fingers can be discriminated with ultrahigh-density diffuse optical tomography," Neuroimage **59**(4), 3201–3211 (2012).
14. I. Nissilä, T. Noponen, K. Kotilahti, T. Katila, L. Lipiäinen, T. Tarvainen, M. Schweiger, and S. Arridge, "Instrumentation and calibration methods for the multichannel measurement of phase and amplitude in optical tomography," Rev. Sci. Instrum. **76**(4), 044302 (2005).
15. H. Dehghani, B. R. White, B. W. Zeff, A. Tizzard, and J. P. Culver, "Depth sensitivity and image reconstruction analysis of dense imaging arrays for mapping brain function with diffuse optical tomography," Appl. Opt. **48**(10), D137–D143 (2009).
16. J. Heiskala, M. Pollari, M. Metsäranta, P. E. Grant, and I. Nissilä, "Probabilistic atlas can improve reconstruction from optical imaging of the neonatal brain," Opt. Express **17**(17), 14977–14992 (2009).
17. M. Cope, "The application of near infrared spectroscopy to non invasive monitoring of cerebral oxygenation in the newborn infant," Ph.D. Thesis (University College London, Department of Medical Physics and Bioengineering, 1991).
18. Y. Yamashita, A. Maki, and H. Koizumi, "Wavelength dependence of the precision of noninvasive optical measurement of oxy-, deoxy-, and total-hemoglobin concentration," Med. Phys. **28**(6), 1108–1114 (2001).
19. C. R. Genovese, N. A. Lazar, and T. Nichols, "Thresholding of statistical maps in functional neuroimaging using the false discovery rate," Neuroimage **15**(4), 870–878 (2002).
20. J. C. Hebden, F. M. Gonzalez, A. Gibson, E. M. C. Hillman, R. M. Yusof, N. Everdell, D. T. Delpy, G. Zaccanti, and F. Martelli, "Assessment of an in situ temporal calibration method for time-resolved optical tomography," J. Biomed. Opt. **8**(1), 87–92 (2003).
21. D. A. Boas, G. Strangman, J. P. Culver, R. D. Hoge, G. Jasdzewski, R. A. Poldrack, B. R. Rosen, and J. B. Mandeville, "Can the cerebral metabolic rate of oxygen be estimated with near-infrared spectroscopy?" Phys. Med. Biol. **48**(15), 2405–2418 (2003).
22. J. P. Kuhtz-Buschbeck, R. Gilster, S. Wolff, S. Ulmer, H. Siebner, and O. Jansen, "Brain activity is similar during precision and power gripping with light force: an fMRI study," Neuroimage **40**(4), 1469–1481 (2008).
23. S. G. Costafreda, C. H. Y. Fu, L. Lee, B. Everitt, M. J. Brammer, and A. S. David, "A systematic review and quantitative appraisal of fMRI studies of verbal fluency: role of the left inferior frontal gyrus," Hum. Brain Mapp. **27**(10), 799–810 (2006).
24. S. Heim, S. B. Eickhoff, and K. Amunts, "Specialisation in Broca's region for semantic, phonological, and syntactic fluency?" Neuroimage **40**(3), 1362–1368 (2008).
25. P. Hiltunen, S. Särkkä, I. Nissilä, A. Lajunen, and J. Lampinen, "State space regularization in the nonstationary inverse problem for diffuse optical tomography," Inverse Probl. **27**(2), 025009 (2011).
26. J. Heiskala, P. Hiltunen, and I. Nissilä, "Significance of background optical properties, time-resolved information and optode arrangement in diffuse optical imaging of term neonates," Phys. Med. Biol. **54**(3), 535–554 (2009).
27. M. A. Franceschini, S. Fantini, J. H. Thompson, J. P. Culver, and D. A. Boas, "Hemodynamic evoked response of the sensorimotor cortex measured noninvasively with near-infrared optical imaging," Psychophysiology **40**(4), 548–560 (2003).

1. Introduction

Near-infrared spectroscopy (NIRS) utilizes light for noninvasively recording blood oxygenation and volume changes in tissue. It is often applied to measure, through the scalp and skull, cerebral hemodynamic changes related to neuronal activity. Its sensitivity to physiologically important parameters, high temporal resolution, portability, inexpensiveness, and safety make the method a compelling alternative to other hemodynamic imaging modalities such as functional magnetic resonance imaging (fMRI) and positron emission tomography. However, besides cerebral hemodynamics, the technique is also sensitive to scalp circulation [1], which is controlled by the autonomic nervous system directly [2,3] and through heart rate and blood pressure indirectly [4]. As stress-related cardiovascular and extracerebral changes are related, the extracerebral effects are expected to show a dependency on heart rate or other cardiovascular parameters. Supporting this view, changes in mean arterial blood pressure and heart rate, as well as pulse magnitude in the scalp measured with laser Doppler flowmetry have been shown to correlate with NIRS signals and the NIRS signals have been shown to contain contribution from extracerebral layers [4–7]. Thus, the

#178634 - $15.00 USD Received 26 Oct 2012; revised 28 Jan 2013; accepted 7 Feb 2013; published 13 Feb 2013

interpretation of NIRS is complicated by scalp and systemic circulation, especially in tasks with increased mental or physical effort.

NIRS can be extended to three-dimensional (3D) imaging with an image reconstruction algorithm if the tissue is probed with overlapping measurements of multiple source-to-detector separations [8]. This technique is known as diffuse optical tomography (DOT). DOT reconstructs images that are technically 3D and can thus, in theory, provide separation between extracerebral physiology and cerebral hemodynamic responses [9]. In practice, the ability to discriminate between changes occurring at different depths is limited. To improve the depth discrimination of DOT, high-density probes and coaxial fibers operating simultaneously as sources and detectors have been used in recent studies [10–13]. Furthermore, signal-processing methods, such as the superficial signal regression (SSR), have been proposed to reduce extracerebral and global systemic variation in the data [11].

In this study, we examine how extracerebral changes triggered by mental and physical stress during task performance affect DOT reconstructions. We investigate and compare experimental and simulated data of cerebral and extracerebral changes to elucidate the effect of scalp circulation on reconstructions of cerebral hemodynamics. We also evaluate the performance of SSR for reducing extracerebral contribution. Furthermore, we use simulations to test the potential benefits of increased measurement density by replacing each source and detector fiber with a coaxial fiber in enhancing the sensitivity and specificity of the reconstructions to cerebral hemodynamics.

2. Methods

2.1 Subjects and tasks

Fourteen healthy, right-handed, Finnish-speaking subjects (ages: 23–34, mean 28; 3 female) participated in two similar measurement sessions on two separate days subsequent to signing an informed consent. One of the two sessions of one subject was rejected because of technical difficulties with the NIRS recording. The study was accepted by the Ethics Committee of Helsinki University Central Hospital and was in compliance with the Declaration of Helsinki.

To induce different levels of mental and physical stress, the subjects performed weekday-recitation, verbal-fluency, and hand-motor tasks during two similar sessions (Fig. 1(a)). Each session included also transcranial magnetic stimulation (TMS) which was related to another study. The subjects performed first alternating hand-motor and weekday-recitation tasks (performed 5 times in total; see Fig. 1(a)) and then verbal-fluency tasks (6 repetitions) in each session. Thereafter, TMS pulses were delivered to the right prefrontal cortex (real TMS) or to the vertex (sham TMS, induced current direction along the interhemispheric fissure) at 1 Hz for about 20 min. Subsequent to TMS, the subjects performed verbal-fluency tasks (6 repetitions) and finally alternating hand-motor and weekday-recitation tasks (5 times in total; see Fig. 1(a)). The post-TMS hand-motor and weekday-recitation tasks were included in the analysis to maximize the amount of data. The post-TMS verbal-fluency tasks were excluded in order to keep the number of repetitions for each task approximately the same. This set was selected not to be analyzed because the TMS protocol was designed to have an effect on the verbal-fluency task even though no significant changes in task performance were observed (the effect of TMS on the verbal-fluency data is beyond the scope of this study).

The hand-motor task consisted of repeatedly and strongly squeezing a hand gripper for 30 s in a self-paced manner (Fig. 1(b)). The verbal-fluency task consisted of a 15-s pre-task period, a 30-s task period, and a 30-s post-task period. During the pre- and post-task periods, the subjects recited weekdays in a consecutive manner. During the task period, they had to name as many words as they could starting with a given letter. The order of the letters was randomized separately for each measurement session. The weekday-recitation task was similar to the verbal-fluency task except during the task period that consisted of reciting weekdays.

Tasks were performed in Finnish, and cues were given visually on a computer screen. Between tasks, resting periods of 42–64 s (verbal fluency), 42–48 s (weekday recitation) or

#178634 - $15.00 USD Received 26 Oct 2012; revised 28 Jan 2013; accepted 7 Feb 2013; published 13 Feb 2013

50–60 s (hand motor) were held. The subjects were instructed to move as little as possible during the tasks in order to minimize the contribution of motion artifacts.

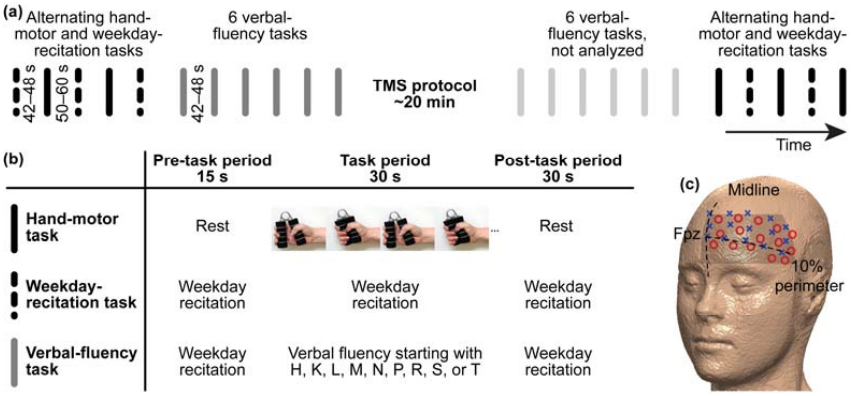

Fig. 1. (a) Task protocol of one measurement session, (b) task description, and (c) positioning of the DOT probe (digitized optode locations of one subject overlaid over the surface rendering of the subject's MRI). Sources are marked with blue crosses and detectors with red circles. The midline and the 10% perimeter according to the International 10–20 system are depicted with dashed lines. The area presented in the results is shaded.

2.2 Measurements

Frequency-domain NIRS data were obtained from the subjects sitting on a chair in a dimly lit room. The NIRS instrument guided intensity-modulated light from two time-multiplexed laser diodes (785 and 824 nm) through optical fibers into the tissue and recorded the attenuation of the modulation amplitude and the phase delay arising in the tissue [14]. The high-density fiber-optic DOT probe was attached on the left side of the forehead according to the International 10–20 system so that the lowest medial source was at Fpz and the lowest row of sources followed the 10% perimeter (Fig. 1(c)). The probe consisted of three rows of five detector fiber bundles and three rows of five source fibers interleaved in a regular pattern and cast in silicone to keep the interoptode distances and terminal angles constant, yet giving the probe flexibility. The signals up to the fourth nearest-neighbor channels (12-, 27-, 36-, and 43-mm source-to-detector separation) were analyzed. The shortest channels record photons travelled mainly in the extracranial layer, whereas in the longer channels relatively more photons have reached the brain tissue as well [15]. The signal-to-noise ratio of longer than 43-mm channels was low; these were therefore not included in the analysis.

Anatomical MRIs of subjects were acquired to digitize and coregister the optode locations in the individual anatomy with MRI-guided eXimia Navigated Brain Stimulation system (Nexstim Ltd., Helsinki, Finland). In the second session, the probe was placed at the same location as in the first session with the help of the navigation system.

To monitor systemic cardiovascular changes, beat-to-beat heart rate was recorded from one subject with an electrocardiogram in one session and with a photoplethysmograph in the other sessions (S/5 patient monitor, Datex-Ohmeda, Finland).

An accelerometer attached to the DOT probe was used for movement detection. In five sessions, the accelerometer data could not be recorded because of technical issues.

2.3 Signal processing

The modulation amplitude detected after light propagation through the tissue was resampled from the original sampling rate of approximately 0.5 Hz to a sampling rate of 1 Hz, high-pass filtered (cutoff: 0.005 Hz) to reduce instrumental drift, and low-pass filtered (0.22 Hz) to

#178634 - $15.00 USD Received 26 Oct 2012; revised 28 Jan 2013; accepted 7 Feb 2013; published 13 Feb 2013

attenuate high-frequency noise. Data corresponding to individual task repetitions were baseline-corrected by setting the mean of the resting data in the time window −10…−1 s prior to task onset to zero (prior to task period in hand motor task and prior to pre-task period in weekday-recitation and verbal-fluency tasks). Artifacts were rejected from the analysis by visual inspection of the NIRS and accelerometer data. Channels were rejected from the analysis if the natural logarithm of their mean variance over all subjects exceeded the value −4, as they most likely had a poor contact (total of 28 out of 162 channels were rejected; 22 of these were 43-mm channels).

The attenuation time series were analyzed with and without SSR. In the SSR algorithm, the average time course over the first nearest-neighbor channels was fitted to the time course of each channel and subtracted prior to calculating DOT reconstructions to reduce global and extracerebral contribution [11].

The NIRS data during separate task repetitions were sorted by the mean heart-rate change at the end of the task period (15…30 s) and grouped into three equal numbered groups within each task. Group "small" consisted of repetitions with the smallest heart-rate changes, group "large" of repetitions with the largest changes, and group "intermediate" of the remaining repetitions.

2.4 Diffuse optical tomography

DOT images of absorption changes in the tissue were reconstructed from the light-attenuation data separately for each task repetition. The sensitivity relation between the measurement and the change in the absorption coefficient in the tissue for each voxel was obtained from a Monte Carlo simulation in a homogeneous head model. The external shape of the head model and the optode positions were derived from the MRI and digitized optode locations of one subject. The following background optical properties were used in the simulation: absorption coefficient $\mu_a = 0.017$ mm^{-1}, reduced scattering coefficient $\mu_s' = 1.1$ mm^{-1}, anisotropy factor $g = 0.8$, and refractive index $n = 1.4$. In addition to this homogeneous head model, also a 5-layered head model (scalp $\mu_a = 0.016$ mm^{-1}, $\mu_s' = 1.4$ mm^{-1}; skull $\mu_a = 0.024$ mm^{-1}, $\mu_s' = 1.25$ mm^{-1}; cerebrospinal fluid $\mu_a = 0.004$ mm^{-1}, $\mu_s' = 0.025$ mm^{-1}; gray matter $\mu_a = 0.0186$ mm^{-1}, $\mu_s' = 0.61$ mm^{-1}; white matter $\mu_a = 0.014$ mm^{-1}, $\mu_s' = 1.1$ mm^{-1}; $g = 0.8$ and $n = 1.4$ for all layers) was created from the same MRI. As reconstructions with this 5-layered model were qualitatively similar to those obtained with the homogeneous model, results only with the homogeneous model are presented in this article. The Monte Carlo method is explained in detail elsewhere [16].

The reconstruction was performed with Tikhonov regularization by minimizing, separately for each time point, the functional

$$\left\|\Delta y - J\Delta x\right\|^2 + \alpha\left\|L\Delta x\right\|^2 \quad (1)$$

where Δy is the measurement data, Δx the differential absorption coefficient to be reconstructed, J the sensitivity matrix, α the regularization parameter ($\alpha_{\text{low}} = 5$ and $\alpha_{\text{high}} = 10^3$ used in this study) and L the discrete Laplace operator. Phase data were not utilized because of their low signal-to-noise ratio when switching detector gains rapidly as in this study.

Reconstructed changes in the absorption coefficient at the two wavelengths were converted into hemoglobin concentration changes with the specific extinction coefficients of oxy- and deoxyhemoglobin [17]. The sum of oxy- and deoxyhemoglobin concentrations ([HbO_2] and [HbR]), i.e., the total hemoglobin concentration ([HbT]), is presented in the results section, since the light wavelengths were not optimal for separating [HbO_2] and [HbR] because of crosstalk [18]. The results for [HbO_2] and [HbR] are included in the Appendix.

To separately visualize the reconstructed changes of [HbT] (Δ[HbT]) in the brain and in the scalp, the voxel data were projected into the intra- and extracranial layers. For the intracranial projection, Δ[HbT] was averaged from a depth of 0 to 5 mm below the skull, and for the extracranial projection, it was averaged from the head surface to a depth of 4 mm. The

#178634 - $15.00 USD Received 26 Oct 2012; revised 28 Jan 2013; accepted 7 Feb 2013; published 13 Feb 2013

projections were averaged over task repetitions and over time steps in the following three time windows: baseline (resting data from −10 to −1 s prior to task onset), task (15…30 s with respect to task period onset), and post-task (45…60 s) periods.

2.5 Statistical testing

Projections and time courses are presented as averages over task repetitions; the reliability of the averages is depicted with the standard error of the mean (SEM) or the 95% confidence interval of the mean obtained from *t*-statistics. The uncorrected significance level of all statistical tests was set at 0.05.

To test the effect of TMS on the DOT projections, projections calculated from repetitions of sham and real TMS sessions were compared pixel by pixel with two-sample *t*-tests. The *p*-values were adjusted for multiple comparisons by controlling the false discovery rate (FDR) over the pixels of the intra- and extracranial projections [19].

Task-related heart-rate changes (mean over 15…30 s of the task period) were tested with two-way analysis of variance (ANOVA) for dependence on factors 'task' (levels: weekday recitation, verbal fluency, hand motor) and 'heart-rate group' (small, intermediate, large). Post-hoc testing of significant two-way interaction was performed with one-way ANOVAs. Significant one-way ANOVAs were further followed up with Tukey–Kramer post-hoc tests. The post-hoc one-way ANOVAs were Bonferroni-corrected for multiple comparisons with factor three.

To test the statistical significance of Δ[HbT] in the projections during the task period, they were compared with baseline projections pixel by pixel with paired *t*-tests. The *p*-values were adjusted for pixelwise multiple comparisons by controlling the FDR over the pixels of the intra- and extracranial projections. The results of these *t*-tests are presented as statistical *t*-maps, where *t*-values exceeding the threshold for statistical significance are colored.

To quantify the heart-rate dependency of Δ[HbT], the projections of the task period were tested pixel by pixel with one-way ANOVA for the continuous factor average heart-rate change. The *p*-values were adjusted for multiple comparisons by controlling the FDR over pixels of the intra- and extracranial projections. The results are presented as *F*-maps, where *F*-values exceeding the level of statistical significance are colored.

2.6 Simulations

To understand our observations and the limitations of DOT in separating cerebral and extracerebral changes, we simulated measurements with cerebral and extracerebral perturbations. We applied two virtual DOT probes: a probe similar to the one used in the measurements ("measurement probe") and another probe with an identical fiber array, but each source and detector replaced with a hybrid optode functioning both as a source and a detector ("hybrid probe") [20]. The measurement probe had 162 and the hybrid probe 642 active channels, as all channels with source-to-detector separations from 0 to 43 mm were included in the analysis.

Five simulated data sets were generated with the following details: (1) a local transient Δ[HbT] in the gray matter, representing cerebral activity (step function in time and space; size 10 mm × 10 mm × depth of gray matter ~3 mm; magnitude 4 μM, Fig. 2(a)); (2) a homogeneous Δ[HbT] in the scalp covering the whole measurement area, representing an extracerebral change (step function in time; depth ~3 mm; activation at the same time as for the local simulated Δ[HbT]; magnitude 4 μM); (3) combined (1) and (2) to simulate simultaneous cerebral and extracerebral changes; (4) as (3), but with a homogeneous extracerebral change of only 0.8 μM; (5) as (4), but with a negative extracerebral change of 0.8 μM.

The simulated data were generated by multiplying a pre-calculated sensitivity matrix with the absorption changes corresponding to the above-introduced simulated changes. The sensitivity matrix was obtained from a Monte Carlo simulation in the 5-layered head model created from the MRI of one subject [16]. Zero-mean white Gaussian noise was added to the simulations prior to calculating the reconstructions. The standard deviation (SD) of the noise

#178634 - $15.00 USD Received 26 Oct 2012; revised 28 Jan 2013; accepted 7 Feb 2013; published 13 Feb 2013

was obtained from the experimental signals: All values of the resting data −10…0 s prior to the task onset were pooled together. The SD was calculated separately for each source-to-detector separation over the pooled values and an exponential function was fitted to the SD estimates (Fig. 2(b)). The SD for the simulated noise was taken from the fitted function separately for each source-to-detector separation and divided by the square root of the number of repetitions to obtain a noise level similar to the averaged responses in the measured data (the SD was calculated over non-averaged data).

The reconstructions of the simulated data were calculated in the same manner as for the measured physiological data using the homogeneous head model. Separate head models were applied for generating the simulated data and performing the reconstructions.

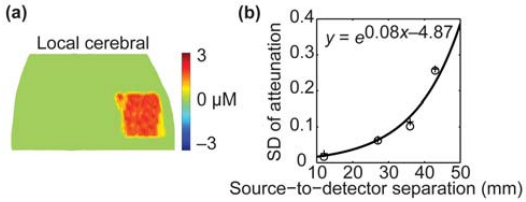

Fig. 2. (a) Simulated cerebral change (intracranial projection; corresponds to the shaded area in Fig. 1(c) on the brain surface) and (b) SD of the experimental resting data as a function of the source-to-detector separation (circle: 824 nm, cross: 785 nm) and the fitted exponential function which was utilized for calculating the SD of the simulated noise.

3. Results

3.1 Effect of TMS on the hand-motor and weekday-recitation tasks

The DOT projections in hand-motor and weekday-recitation tasks did not show statistically significant differences between sham and real TMS sessions (see Appendix). Even without any adjustment to the *p*-values, less than 1% of the pixels exceeded the limit of statistical significance. In the following analysis we assume that the effect of TMS on the DOT data was negligible.

3.2 Heart rate

The heart rate increased during all tasks (Fig. 3); the average increase differed significantly between the heart-rate groups (Fig. 4). The weekday-recitation task showed the lowest and the hand-motor task the highest heart-rate changes, except in the heart-rate group "small" where the verbal-fluency and hand-motor task did not differ significantly. The average heart-rate increases were 6 ± 4 beats per minute (bpm) in the weekday-recitation task (mean over repetitions ± SD), 11 ± 6 bpm in the verbal-fluency task, and 15 ± 9 bpm in the hand-motor task.

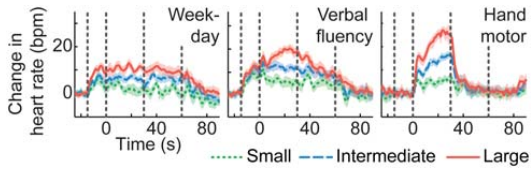

Fig. 3. Averaged heart-rate time series in separate tasks and heart-rate groups. Vertical dashed lines indicate start of the pre-task, start and end of the task, and end of the post-task period. Shading depicts the 95% confidence interval of the mean.

#178634 - $15.00 USD Received 26 Oct 2012; revised 28 Jan 2013; accepted 7 Feb 2013; published 13 Feb 2013

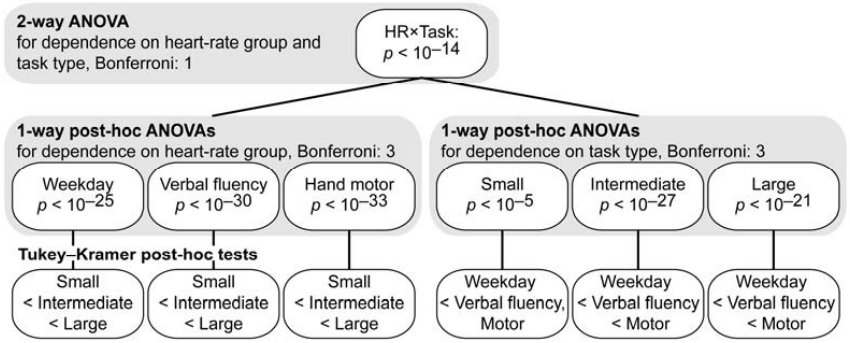

Fig. 4. Two-way ANOVA and post-hoc tests for the heart-rate change. Interaction between factors X and Y is marked with $X \times Y$. For all Tukey–Kramer results, $p < 10^{-4}$. The heart-rate change differed significantly between the heart-rate groups (HR) and tasks, except in the group "small", where verbal-fluency and hand-motor task did not differ significantly.

3.3 DOT data

In the extracranial projections of the DOT reconstructions, [HbT] changed during the hand-motor and verbal-fluency tasks (Fig. 5, Media 1). The hand-motor task produced a strong positive Δ[HbT] during the task period over most of the sensitivity area of the measurement. This change was stronger in heart-rate groups "intermediate" and "high" than in the group "small". The dependency on the heart rate was statistically significant in 11% of the extracranial pixels. The verbal-fluency task produced more complex features in the extracranial projections during the task period. The groups "small" and "intermediate" showed an overall positive change in the measured volume and the group "large" mainly a negative change. Of all the extracranial pixels, 32% showed a significant dependence on the heart rate. During the post-task period of the verbal-fluency task, a wide positive change occurred. The weekday task showed barely any significant Δ[HbT] during the task period and did not depend on the heart rate.

The intracranial projections exhibited also changes during the hand-motor and verbal-fluency tasks. In both tasks, a positive change was visible in the approximate location of the pars triangularis in the inferior frontal gyrus during the task period (Fig. 5, Media 1). This positive change did not depend significantly on the heart rate either in the hand-motor or the verbal-fluency task. However, the hand-motor task showed a tendency towards smaller Δ[HbT] in the heart rate group "small" as compared to the other groups. Furthermore, the location of this change varied slightly between the heart-rate groups. In addition to this lateral Δ[HbT], both tasks showed weak negative changes more centrally. Moreover, the motor task produced positive changes at the edges of the sensitivity area of the measurement, especially in the "intermediate" and "large" groups. The wide post-task change seen in the extracranial projection in the verbal-fluency task was not visible in the intracranial projection.

#178634 - $15.00 USD Received 26 Oct 2012; revised 28 Jan 2013; accepted 7 Feb 2013; published 13 Feb 2013

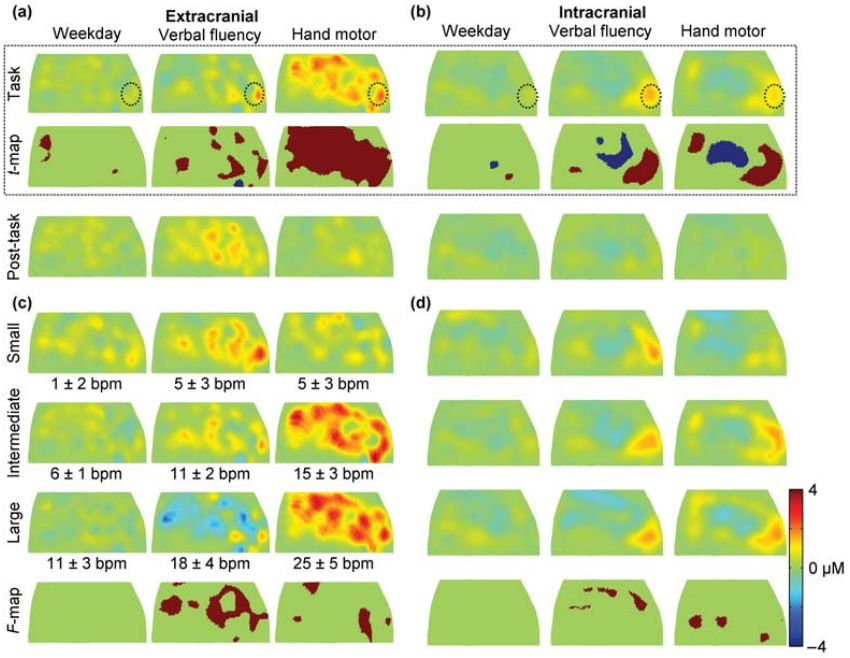

Fig. 5. (a, c) Extra- and (b, d) intracranial projections of reconstructed Δ[HbT] with the regularization parameter α_{low} (a, b) averaged over task repetitions during the task and post-task periods (whole time course shown in Media 1), or (c, d) averaged over repetitions in specific heart-rate groups during the task period. The projections represent the shaded area in Fig. 1(c) on the scalp (extracranial) or brain surface (intracranial). In (a, b), also statistical *t*-maps are presented, indicating statistically significant Δ[HbT] during task period with respect to baseline (positive: red; negative: blue). In (c, d) *F*-maps for the dependence on heart rate are presented. Average heart-rate changes ± SD in the heart-rate groups are indicated also in (c). The average location of pars triangularis is marked with a dotted circle (radius: SD over subjects). In the extracranial projections, the hand-motor task produced the strongest and the weekday-recitation task the weakest Δ[HbT], which depended on the heart rate in the hand-motor and verbal-fluency tasks. Both the verbal-fluency and hand-motor tasks showed also an increase in [HbT] in the intracranial layer located approximately in the pars triangularis.

SSR removed the wide changes visible in the extracranial projections during the hand-motor and verbal-fluency tasks (Fig. 6), although some significant changes remained in the extracerebral layers. SSR made the extracranial projections in the separate heart-rate groups more alike. Furthermore, it attenuated the extracranial Δ[HbT] during the post-task period of the verbal-fluency task. The intracranial projections were affected less by SSR. The lateral positive Δ[HbT] remained in the intracranial projections of the hand-motor and verbal-fluency tasks even after SSR. The positive Δ[HbT] around the edges of sensitivity area were, nevertheless, attenuated in the hand-motor task.

#178634 - $15.00 USD Received 26 Oct 2012; revised 28 Jan 2013; accepted 7 Feb 2013; published 13 Feb 2013

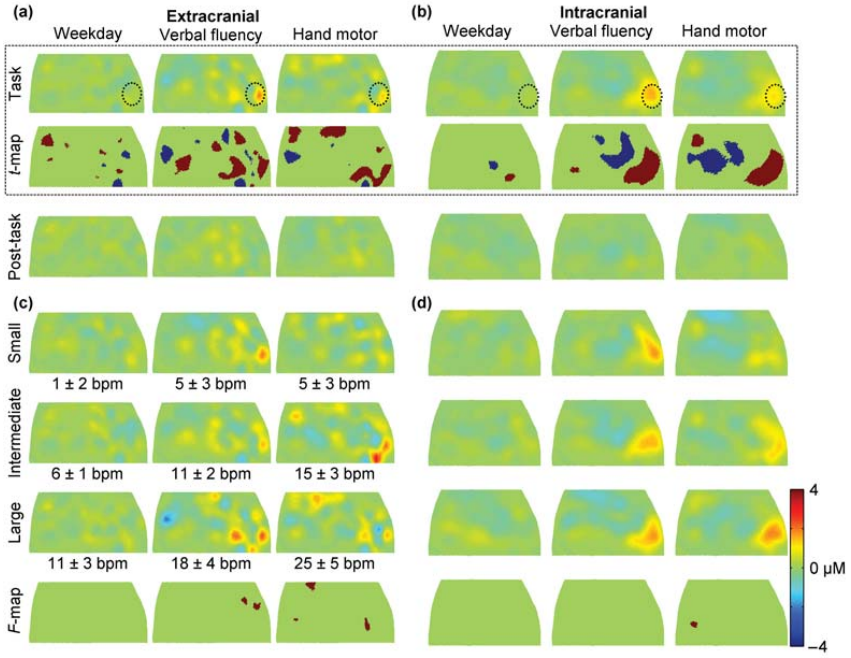

Fig. 6. Cases as in Fig. 5, but after SSR. SSR attenuates strong changes in the extracranial layers and the heart-rate dependency of almost all pixels.

Reconstructions with the 5-layered head model were qualitatively similar to the ones obtained with the homogeneous model (Appendix), except that the lateral intracranial Δ[HbT] depended statistically significantly on the heart rate during the hand-motor task. The higher regularization parameter smoothed the reconstructions, making the extra- and intracranial reconstructions more similar to each other (Appendix). The projections of [HbO_2] and [HbR] showed changes in locations comparable to Δ[HbT] (Appendix). However, [HbR] changed statistically significantly only during the verbal-fluency task.

3.4 Simulated data

A simulated local cerebral change (set 1, Fig. 2(a)) was reconstructed in the correct position on the cortical surface (Fig. 7(a)), albeit with a reduced magnitude. The reconstruction of a positive homogeneous extracerebral change (set 2) indicated crosstalk between layers: changes were visible in the intracranial layer as well (Fig. 7(b)), although the simulated Δ[HbT] was located in the scalp. The shape of the crosstalk depended on the choice of the regularization parameter. With α_{low}, mainly negative Δ[HbT] arose in the middle of the intracranial projections and positive Δ[HbT] on the edges of the probed area; this results from a denser sampling in the middle of the probe as compared to the sides. With α_{high}, the positive Δ[HbT] spread into the intracranial layer.

In the reconstruction of combined extracerebral and local cerebral changes (set 3), the extracerebral change dominated over the cerebral change, and the extracerebral and cerebral components could not be clearly separated even with the hybrid probe (Fig. 7(c)). The localized cerebral change became visible in the reconstruction when the positive (set 4, Fig. 7(d)) or negative (set 5, Fig. 7(e)) extracerebral change was about 20% of the strength of the cerebral change.

#178634 - $15.00 USD Received 26 Oct 2012; revised 28 Jan 2013; accepted 7 Feb 2013; published 13 Feb 2013

SSR was able to remove the homogeneous extracerebral change and the related crosstalk between layers (set 2, Fig. 7(b)), but when the cerebral and extracerebral changes correlated in time and shape, SSR also removed the cerebral Δ[HbT] (sets 3–5, Figs. 7(c)–7(e)).

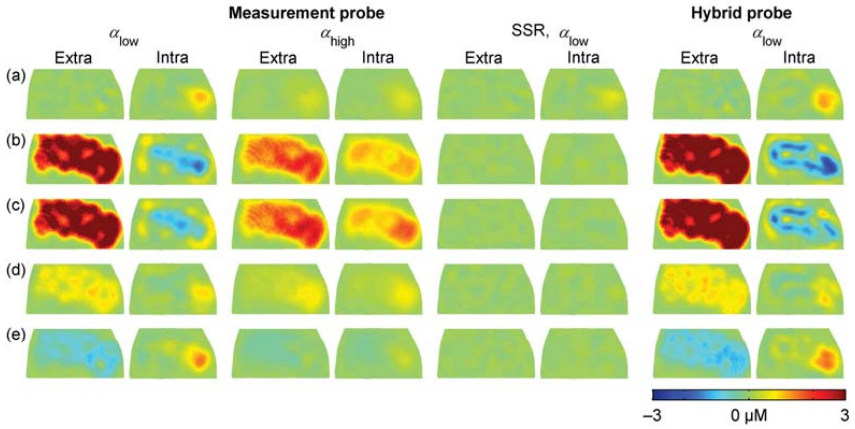

Fig. 7. Δ[HbT] reconstructed from simulated data with regularization parameters α_{low} and α_{high} and projected into the extra- and intracranial layers (marked with Extra and Intra). The reconstructions with α_{low} were also calculated after SSR and in a denser hybrid probe that has coaxial sources and detectors. (a) Local cerebral (set 1), (b) homogeneous extracerebral (set 2), (c) local cerebral and strong positive homogeneous extracerebral (set 3), (d) local cerebral and weak positive homogeneous extracerebral (set 4), and (e) local cerebral and weak negative homogeneous extracerebral perturbations (set 5). The projections represent the shaded area in Fig. 1(c).

4. Discussion

This study presents an analysis of DOT reconstructions of hemodynamic changes during three task conditions: (1) a hand-motor task causing a strong task-related change in the extracerebral circulation in the forehead, (2) a verbal-fluency task with likely simultaneous extracerebral and cerebral changes, and (3) a weekday-recitation task showing no significant extracerebral or cerebral task-related changes. Strong changes in the extracerebral circulation affected the intracranial layer of the reconstructions, distorting the reconstructed hemodynamic changes related to brain activity. Analysis of simulated cases indicated crosstalk between the layers, supporting this observation. However, SSR and division of the data into heart-rate groups helped in identifying cerebral hemodynamic activity related to the verbal-fluency task. During the hand-motor task, the extracerebral changes were stronger, making the identification of cerebral components less clear.

The hand-motor task invoked a strong change in the heart rate and a spatially broad increase in the reconstructed extracranial [HbT]. This extracranial Δ[HbT] was mostly removed by SSR, which attenuates variation common to all superficially sensitive channels. SSR also removed the dependency of this extracranial Δ[HbT] on the heart rate, which is a rough indicator of the strength of the task-related stress response and is expected to correlate with extracerebral changes. These results, together with the fact that the intracranial Δ[HbT] resembled the simulated crosstalk artifact between layers, indicate that the extracranial Δ[HbT] during the hand-motor task was caused by changes in the extracerebral circulation. This observed increase in the extracerebral blood volume (proportional to [HbT] [21]) is also consistent with physiological changes during physical exercise: the small arteries in the scalp of the forehead dilate in response to increased body temperature to cool down the tissue [3].

The verbal-fluency task also elicited changes in the heart rate and the extracranial [HbT]. During the post-task period, Δ[HbT] resembled the extracranial changes observed during the

#178634 - $15.00 USD Received 26 Oct 2012; revised 28 Jan 2013; accepted 7 Feb 2013; published 13 Feb 2013

hand-motor task, i.e., it covered most of the probed area, resembled the crosstalk artifact between layers, and was removed by SSR. Thus, this post-task Δ[HbT] appears to be caused by changes in the extracerebral circulation and likely reflects synchronized inhalation at the end of the task. The task period caused changes in the extracranial [HbT] that correlated negatively with the heart rate. A negative correlation between extracerebral changes and heart rate may be attributed to sympathetic vasoconstriction as a consequence of mental stress caused by the task [1]. Thus, it is likely that the observed changes in the extracranial projections during the task period of the verbal-fluency task were mostly related to changes in the extracerebral circulation.

Besides the broad extracranial Δ[HbT], both the hand-motor and verbal-fluency tasks revealed a positive intracranial Δ[HbT] in the lower lateral part of the measured area located approximately at the pars triangularis in the left inferior frontal gyrus. In the hand-motor task, this positive Δ[HbT] somewhat resembled the crosstalk artifact observed in the simulations between layers and its location and strength varied slightly between heart-rate groups; these observations suggest that extracerebral changes were, at least partly, responsible for the observed intracranial Δ[HbT] in the hand-motor task. On the other hand, it is also possible that the lateral change reflected partly brain activity, as the left inferior frontal gyrus (Brodmann area 44) has been shown to be activated in a power-gripping task [22]. In the verbal-fluency task, the positive Δ[HbT] in the intracranial projection did not show heart-rate dependence, was stronger in magnitude than in the extracranial projection and remained after SSR similar in all heart-rate groups. These observations, together with the fact that the inferior frontal gyrus (Brodmann areas 44/45) has been shown to be activated in the verbal-fluency task [23,24], suggest that this positive Δ[HbT] is due to brain activity.

As a control, the weekday-recitation task did not show extensive Δ[HbT] in the intra- or extracranial layers. The heart-rate changes were small as well, indicating minor contribution of task-related stress and thus also less pronounced extracerebral effects. The lack of cerebral hemodynamic activity in the measured region during the weekday-recitation task corresponds to the current understanding of the role of the inferior frontal gyrus; repeating a predefined word does not require semantic or phonological processing, and therefore the inferior frontal gyrus is not active [23].

SSR has been applied in several studies to attenuate global physiological and surface variation components in optical data [10,11]. The current results demonstrate that the method indeed reduces task-related extracerebral effects during the hand-motor and verbal-fluency tasks. The simulations reveal, however, a methodological problem of SSR: if the extracerebral and cerebral changes correlate in time and shape, cerebral activity is eliminated along with extracerebral effects when processing the data with SSR. In the real physiological data of this study, this did, nevertheless, not seem to be the case, as the intracranial changes were not greatly affected by SSR. In contrast, since the possibility of the intracranial changes during the hand-motor task being caused by crosstalk artifacts between layers could not be ruled out, the ability of SSR to remove all extracerebral contribution from the reconstructed brain activations was not fully confirmed.

Since TMS is a method for modifying cortical excitability, it may have, in theory, affected brain activity in post-TMS tasks after real TMS (one quarter of the hand-motor and weekday-recitation tasks). However, the reconstructions between the DOT data measured in sham and real TMS sessions did not show statistically significant differences. Thus the effect, if present, is weak in the DOT data. Moreover, most of the data were recorded before TMS or after sham TMS, and were thus not affected by TMS per se. In addition, the post-TMS hand-motor and weekday-recitation tasks started 10 min after the end of the TMS protocol, toning down the possible effects. Thus, the effect of TMS on the results can be considered negligible in terms of data interpretation.

The data were sampled at approximately 0.5 Hz, and therefore it is possible that the signals include a pulsatile component aliased from the heartbeat. Since the original digitization was not synchronized to the heartbeat or task onset, the time course of the aliased component varies from task repetition to repetition. Therefore, the aliased component was

#178634 - $15.00 USD Received 26 Oct 2012; revised 28 Jan 2013; accepted 7 Feb 2013; published 13 Feb 2013

attenuated by the averaging procedure. Moreover, the aliased component should have the same shape in all layers of the reconstructions, whereas the reconstructions of this study vary between layers. Thus, it is highly unlikely that the reported changes were substantially distorted by the aliased pulsatile component from the heart rate.

The value of the regularization parameter affected the reconstructions because it controls the smoothness of the results. The crosstalk between layers was, however, visible with both regularization parameters tested. Instead of applying the simple Tikhonov regularization as in this study, a Kalman-filter-type regularization should, in theory, improve the signal-to-noise ratio of the reconstructions by smoothing the data also in the time domain [25]. In addition, including measured phase information, when available and of good quality, should make the reconstructions more robust and consistent across individual cases and improve the depth sensitivity further [26].

Reconstructing Δ[HbR] instead of Δ[HbT] might improve the sensitivity to brain activity-related changes [1,27]. However, the laser wavelengths of our instrument were not optimal for separating Δ[HbR] and Δ[HbO_2] [18], and thus Δ[HbR] contained more noise than Δ[HbT]. Nevertheless, Δ[HbR] was significant during the verbal-fluency task, but not during the other tasks, supporting the view that the intracranial changes in the verbal-fluency task were related to cerebral hemodynamic changes. The wavelength selection does not substantially affect the Δ[HbT] reconstructions [18], and thus the reported effects will be present in Δ[HbT] irrespective of the wavelengths utilized in the measurements.

The reconstructions were calculated in the same head model for all subjects; the projections were averaged over subjects pixel by pixel. Individual head models and transforming the data into Talairach coordinates might increase the accuracy of the reconstructions and thus improve the separation of the cerebral and extracerebral components. However, the application of a 5-layered head model did not quantitatively change the results.

Finally, the simulations suggested that the cerebral hemodynamic changes cannot be fully separated even with a hybrid probe of the density and coverage considered in this study. Nevertheless, high-density and hybrid probes have been shown effective in recording brain activity in tasks with less extracerebral contribution [10,12,13].

5. Conclusion

DOT is capable of extracting depth information from NIRS data, but extensive task-related changes in the extracerebral circulation of the forehead affect the intracranial layer of reconstructions, distorting hemodynamic signals related to cerebral activity. Even the recordings with the hybrid probe (optode density: 0.9 cm^{-2}) were affected by the crosstalk artifact between the layers and could not fully distinguish between extracerebral and cerebral changes. Nevertheless, by applying SSR to the data and grouping data according to the simultaneously occurring heart-rate change, we were able to identify hemodynamic changes related to the activity of the left inferior gyrus during a verbal fluency task with reasonable confidence. In a hand-motor task, during which especially strong changes in the extacerebral circulation occurred, such clear separation between extracerebral effects and cerebral activity was not achieved. Since task-related extracerebral effects can affect the DOT reconstructions of hemodynamic changes related to brain activity, their contribution should be taken into account in future studies where a strong systemic response is observed during the task performance either due to physical or mental stress. The effect of the reconstruction algorithm as well as optical probe design on the ability of DOT to discriminate between extra- and intracranial changes requires further study.

Appendix: Supplementary figures

This Appendix contains results of Δ[HbT] reconstructions calculated separately for real- and sham-TMS sessions (Fig. 8), of Δ[HbT] reconstructions calculated with the 5-layered head model (Fig. 9), of Δ[HbT] reconstructions with the higher regularization parameter (Fig. 10), and of Δ[HbO_2] and Δ[HbR] reconstructions (Figs. 11–12).

#178634 - $15.00 USD Received 26 Oct 2012; revised 28 Jan 2013; accepted 7 Feb 2013; published 13 Feb 2013

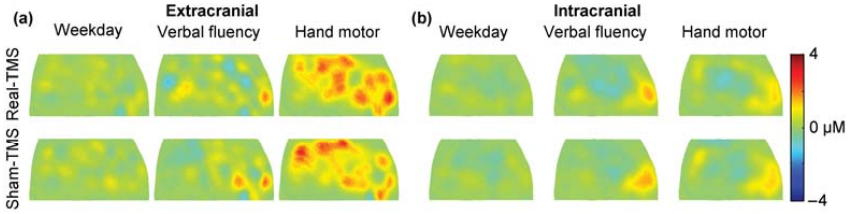

Fig. 8. DOT projections in (a) extra- and (b) intracranial layers during task periods of real and sham TMS sessions. The verbal-fluency task has been performed before TMS. Two-sample *t*-tests showed no statistically significant differences between projections of the two sessions.

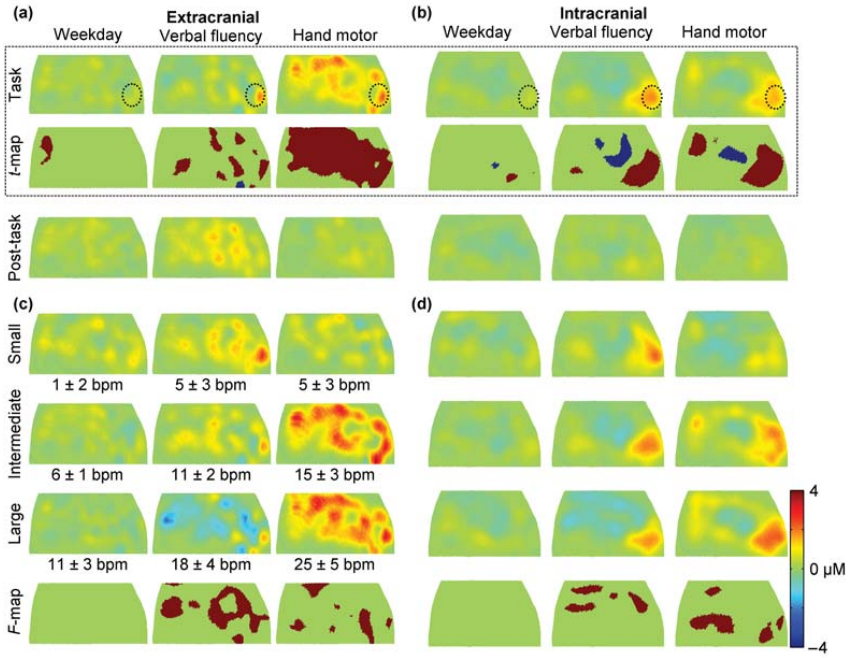

Fig. 9. Cases as in Fig. 5, but reconstructions calculated with the 5-layered head model.

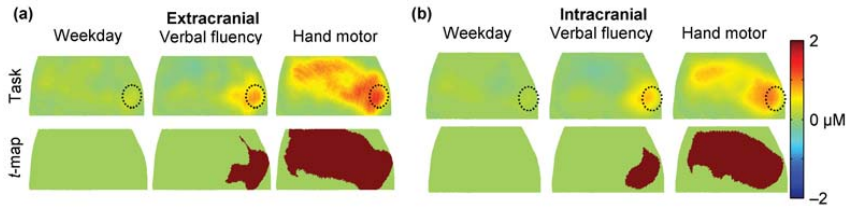

Fig. 10. Cases as in Fig. 5, but reconstructions calculated with α_{high}.

#178634 - $15.00 USD Received 26 Oct 2012; revised 28 Jan 2013; accepted 7 Feb 2013; published 13 Feb 2013

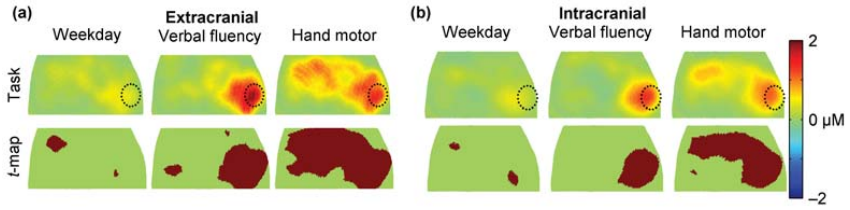

Fig. 11. Cases as in Fig. 5, but for $\Delta[HbO_2]$ and with α_{high}.

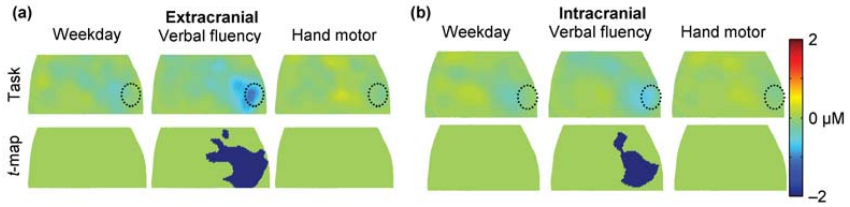

Fig. 12. Cases as in Fig. 5, but for $\Delta[HbR]$ and with α_{high}.

Acknowledgments

We would like to acknowledge the financial support from the Finnish Cultural Foundation, the International Graduate School in Biomedical Engineering and Medical Physics, the Academy of Finland (projects 121167 and 141102), and the European Community's Seventh Framework Programme (FP7/2007-2013) under grant agreement nº201076. We also thank Alexander March for providing help with editing the manuscript.